Unsteady Viscous Flow over Elliptic Cylinders At Various Thickness with Different Reynolds Numbers

Moon-Sang Kim*
Associate Professor, School of Aerospace and Mechanical Engineering, Hankuk Aviation University, Kyungki-Do 412-791, Korea
Ayan Sengupta
Research Assistant, Department of Aerospace Engineering, Iowa State University, Ames, IA 50011, USA

Two-dimensional incompressible Navier-Stokes equations are solved using SIMPLER method in the intrinsic curvilinear coordinates system to study the unsteady viscous flow physics over two-dimensional ellipses Unsteady viscous flows over various thickness-to-chord ratios of 0 6, 0 8, 1 0, and 1 2 elliptic cylinders are simulated at different Reynolds numbers of 200, 400, and 1,000 This study is focused on the understanding the effects of Reynolds number and elliptic cylinder thickness on the drag and lift forces The present numerical solutions are compared with available experimental and numerical results and show a good agreement Through this study, it is observed that the Reynolds number and the cylinder thickness affect significantly the frequencies of the force oscillations as well as the mean values and the amplitudes of the drag and lift forces

Key Words : Unsteady Viscous Flow, Vortex Shedding, SIMPLER Method, Elliptic Cylinder, Navier-Stokes Equations

1. Introduction

The earliest recorded observation of the phenomenon of vortex shedding can be traced back to the sixteenth century when Leonardo da Vinci made drawings of surface pattern of the fluid flow past an obstacle (Perry et al , 1982)

A wake flow behind a bluff body is very significant flow phenomena in the engineering field The alternate vortex shedding occurred in the near wake behind a bluff body leads to periodically oscillating drag and lift forces Especially the oscillating lift force, whose direction is transverse to the flow, is large and may cause structural vibrations, acoustic noise, or resonance, which in some cases can trigger failure (Williamson, 1996)

Many researcher have studied steady/unsteady flows past over circular cylinders Park et al (1998) reported detailed information of flow quantities on the cylinder surface at low Reynolds numbers up to 160 A detailed study of the wake structures and flow dynamics associated with simulated two-dimensional flows past a circular cylinder that is either stationary or in simple harmonic cross-flow oscillation is done by Blackburn and Henderson (1999) Jordan and Fromm (1972) investigated oscillatory drag, lift, and torque on a circular cylinder in a uniform flow at Reynolds numbers of 100, 400, and 1,000 by solving vorticity-stream function formulation They showed the dramatic rise of the drag coefficient during the development of the Kármán vortex street Manzari (2003) presented a finite

* Corresponding Author,
E-mail mskim@mail hau ac kr
TEL +82-2-300-0285, **FAX** +82-2-3158-2191
Associate Professor, School of Aerospace and Mechanical Engineering, Hankuk Aviation University, Kyungki-Do 412-791, Korea (Manuscript **Received** August 17, 2004, **Revised** December 31, 2005)

element solution procedure for the simulation of transient incompressible fluid flows using triangular meshes His algorithm is based on the artificial compressibility technique in connection with a dual time-stepping approach A higher-order immersed boundary method was applied to the two-dimensional unsteady incompressible Navier-Stokes equations in vorticity-stream function formulation to solve unsteady incompressible flow by Linnick and Fasel (2003)

Besides the basic study or development of numerical algorithm to solve flows past circular cylinders, some researchers have tried to control the vortex shedding Kang and Choi (1999) investigated two-dimensional laminar flow past a circular cylinder rotating with a constant angular velocity for the purpose of controlling vortex shedding and understanding the underlying flow mechanism Also, Park et al.(1994) studied the feedback control of von Kármán vortex shedding behind a circular cylinder at low Reynolds numbers numerically

Actually, many studies have been accomplished for flows past circular cylinders because of geometric simplicity However, it would be valuable attempts to study the flows past elliptic cylinders Engineering applications often involve flows over complex bodies like wings, submarines, missiles, and rotor blades, which can hardly be modeled as a flow over a circular cylinder In such flows, cylinder thickness and angle of attack can greatly influence the nature of separation and the wake structure (Mittal and Balachandar, 1996)

In 1987, Ota et al (1987) investigated a flow around an elliptic cylinder of axis ratio 1 3 in the critical Reynolds number regime, which extends from about Re=85,000 to 312,000, on the basis of mean static pressure measurements along the cylinder surface and of hot-wire velocity measurements in the near wake Nair and Sengupta (1996) solved Navier-Stokes equations in order to study the onset of computed asymmetry around elliptic cylinders at a Reynolds number of 10,000 They found that the ellipses developed asymmetry much earlier than the circular cylinder Patel (1981), Chou & Huang (1996), Nair & Sengupta (1997), D'Alessio et al.(1999), and Badr et al (2001) solved unsteady Navier-Stokes equations expressed in terms of stream function and vorticity formulations to study the flows past elliptic cylinders for different angles of attack in the range of Reynolds numbers from 100 to 40,000

The objective of the present research is to study the effects of elliptic cylinder thickness and Reynolds numbers on the unsteady flow physics concentrating on the drag and lift forces exerted on the body Unsteady viscous flows over various thickness-to-chord ratios of 0 6, 0 8, 1 0, and 1 2 elliptic cylinders are simulated at different Reynolds numbers of 200, 400, and 1,000 by solving unsteady form of incompressible Navier-Stokes equations, which is written in two-dimensional body intrinsic orthogonal curvilinear coordinate system

For the temporal integration, Crank-Nicolson scheme is used Patankar (1980) showed that the power law scheme ideally fits for all the Peclet numbers, so power law scheme is used for spatial discretization

Current techniques for the solution of incompressible viscous flow can be categorized as vorticity-stream function methods, artificial compressibility methods, and projection methods The projection method is a fractional step method in which an intermediate velocity and pressure are calculated The SIMPLE (Patankar 1980, Patankar and Spalding 1972) method and all related SIMPLE methods fall in this category In this paper, the discretized equations are solved using a segregated approach where the discretized equation for each variable is solved sequentially using SIMPLER method (Patankar, 1980)

2. Governing Equations

2.1 Navier-Stokes equations

For the present analysis, the flowfield is assumed to be a two-dimensional unsteady, incompressible, laminar flow The coordinate system is taken to be a two-dimensional, body-intrinsic, orthogonal curvilinear coordinate system shown in Fig 1 wherein the ξ-direction is taken to be along the body while the η-direction is perpen-

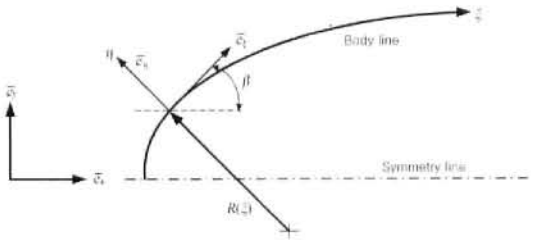

Fig. 1 Two-dimensional body-intrinsic coordinate system

dicular to the body surface. With these assumptions, continuity and momentum equations can be expressed as follows (detailed derivation can be found in Lim 1991):

Continuiy Equation

$$\frac{\partial \rho}{\partial t}+\frac{1}{h_1}\frac{\partial}{\partial \xi}(\rho v_\xi)+\frac{1}{h_1}\frac{\partial}{\partial \eta}(h_1\rho v_\eta)=0 \quad (1)$$

Here, h_1 is scale factor in the ξ-direction. The first term can be dropped for incompressible flow but it is retained here for convenience.

v_ξ-Momentum Equation

$$\begin{aligned}&\frac{\partial}{\partial t}(\rho v_\xi)+\frac{1}{h_1}\frac{\partial}{\partial \xi}\left(\rho v_\xi v_\xi-\frac{1}{h_1}\mu\frac{\partial v_\xi}{\partial \xi}\right)\\&+\frac{1}{h_1}\frac{\partial}{\partial \eta}\left(h_1\rho v_\eta v_\xi-h_1\mu\frac{\partial v_\xi}{\partial \eta}\right)\\&=-\frac{1}{h_1}(\rho v_\xi v_\eta)\frac{\partial h_1}{\partial \eta}-\frac{1}{h_1}\frac{\partial p}{\partial \xi}\\&+\frac{\mu}{h_1}\left[\frac{\partial}{\partial \xi}\left(\frac{v_\eta}{h_1}\frac{\partial h_1}{\partial \eta}\right)+\left(\frac{1}{h_1}\frac{\partial v_\eta}{\partial \xi}-\frac{v_\xi}{h_1}\frac{\partial h_1}{\partial \eta}\right)\frac{\partial h_1}{\partial \eta}\right]\end{aligned} \quad (2)$$

v_η-Momentum Equation

$$\begin{aligned}&\frac{\partial}{\partial t}(\rho v_\eta)+\frac{1}{h_1}\frac{\partial}{\partial \xi}\left(\rho v_\xi v_\eta-\frac{1}{h_1}\mu\frac{\partial v_\eta}{\partial \xi}\right)\\&+\frac{1}{h_1}\frac{\partial}{\partial \eta}\left(h_1\rho v_\eta v_\eta-h_1\mu\frac{\partial v_\eta}{\partial \eta}\right)\\&=-\frac{1}{h_1}(\rho v_\xi v_\xi)\frac{\partial h_1}{\partial \eta}-\frac{\partial p}{\partial \eta}\\&+\frac{\mu}{h_1}\left[\frac{\partial}{\partial \xi}\left(\frac{v_\xi}{h_1}\frac{\partial h_1}{\partial \eta}\right)-\left(\frac{1}{h_1}\frac{\partial v_\xi}{\partial \xi}-\frac{v_\eta}{h_1}\frac{\partial h_1}{\partial \eta}\right)\frac{\partial h_1}{\partial \eta}\right]\end{aligned} \quad (3)$$

2.2 Discretization of governing equations

The surface and time integration of the governing equations over the control volume can be done term by term and expressed as follows in the intrinsic curvilinear coordinate system. All the detailed derivations of the following discretized governing equations can be found in Senguta (2003).

Continuity Equation

$$\begin{aligned}&(\rho-\rho^0)\frac{h_1\Delta\xi\Delta\eta}{\Delta t}+\alpha(F_{i+\frac{1}{2},j}-F_{i-\frac{1}{2},j}+F_{i,j+\frac{1}{2}}-F_{i,j-\frac{1}{2}})\\&+(1-\alpha)(F^0_{i+\frac{1}{2},j}-F^0_{i-\frac{1}{2},j}+F^0_{i,j+\frac{1}{2}}-F^0_{i,j-\frac{1}{2}})=0\end{aligned} \quad (4)$$

where

$$F_{i+\frac{1}{2},j}=(\rho v_\xi)_{i+\frac{1}{2},j}\Delta\eta,\ F_{i-\frac{1}{2},j}=(\rho v_\xi)_{i-\frac{1}{2},j}\Delta\eta$$

$$F_{i,j+\frac{1}{2}}=(h_1\rho v_\eta)_{i,j+\frac{1}{2}}\Delta\xi,\ F_{i,j-\frac{1}{2}j}=(h_1\rho v_\eta)_{i,j-\frac{1}{2}j}\Delta\xi$$

Here, superscript "0" represents the variable quantity at the old time step. The value of $\alpha=0.5$ corresponds to the Crank-Nicolson time integration scheme and $\alpha=1.0$ corresponds to the fully implicit scheme. In this study, Crank-Nicolson scheme was chosen.

v_ξ-Momentum Equation

$$\begin{aligned}&[(\rho v_\xi)-(\rho v_\xi)^0]\frac{h_1\Delta\xi\Delta\eta}{\Delta t}\\&+\alpha\left(J_{v_{\xi_{i-\frac{1}{2},j}}}-J_{v_{\xi_{i-\frac{1}{2},j}}}+J_{v_{\xi_{i,j-\frac{1}{2}}}}-J_{v_{\xi_{i,j-\frac{1}{2}}}}\right)\\&+(1-\alpha)\left(J^0_{v_{\xi_{i-\frac{1}{2},j}}}-J^0_{v_{\xi_{i-\frac{1}{2},j}}}+J^0_{v_{\xi_{i,j-\frac{1}{2}}}}-J^0_{v_{\xi_{i,j-\frac{1}{2}}}}\right)\\&=(\alpha S_{v_\xi}+(1-\alpha)S^0_{v_\xi})_{i,j}h_1\Delta\eta+(p_{i-1,j}-p_{i,j})h_1\Delta\eta\end{aligned} \quad (5)$$

where

$$J_{v_\xi\xi}=\left(\rho v_\xi v_\xi-\frac{1}{h_1}\mu\frac{\partial v_\xi}{\partial \xi}\right)\Delta\eta$$

$$J_{v_\xi\eta}=\left(h_1\rho v_\xi v_\eta-h_1\mu\frac{\partial v_\xi}{\partial \eta}\right)\Delta\xi$$

$$\begin{aligned}S_{v_\xi}=&-\frac{1}{h_1}(\rho v_\xi v_\eta)\frac{\partial h_1}{\partial \eta}+\frac{\mu}{h_1}\left[\frac{\partial}{\partial \xi}\left(\frac{v_\eta}{h_1}\frac{\partial h_1}{\partial \eta}\right)\right.\\&\left.+\left(\frac{1}{h_1}\frac{\partial v_\eta}{\partial \xi}-\frac{v_\xi}{h_1}\frac{\partial h_1}{\partial \eta}\right)\frac{\partial h_1}{\partial \eta}\right]\end{aligned}$$

u_η-Momentum Equation

$$\begin{aligned}&[(\rho v_\eta)-(\rho v_\eta)^0]\frac{h_1\Delta\xi\Delta\eta}{\Delta t}\\&+\alpha\left(J_{v_{\eta_{i-\frac{1}{2},j}}}-J_{v_{\eta_{i-\frac{1}{2},j}}}+J_{v_{\eta_{i,j-\frac{1}{2}}}}-J_{v_{\eta_{i,j-\frac{1}{2}}}}\right)\\&+(1-\alpha)\left(J^0_{v_{\eta_{i-\frac{1}{2},j}}}-J^0_{v_{\eta_{i-\frac{1}{2},j}}}+J^0_{v_{\eta_{i,j-\frac{1}{2}}}}-J^0_{v_{\eta_{i,j-\frac{1}{2}}}}\right)\\&=(\alpha S_{v_\eta}+(1-\alpha)S^0_{v_\eta})_{i,j}h_1\Delta\xi\Delta\eta+(p_{i,j-1}-p_{i,j})h_1\Delta\xi\end{aligned} \quad (6)$$

where

$$J_{v_\xi\xi}=\left(\rho v_\eta v_\xi-\frac{1}{h_1}\mu\frac{\partial v_\xi}{\partial\xi}\right)\Delta\eta$$

$$J_{v_\eta\eta}=\left(h_1\rho v_\eta v_\eta-h_1\mu\frac{\partial v_\eta}{\partial\eta}\right)\Delta\xi$$

$$S_{v_\eta}=-\frac{1}{h_1}(\rho v_\xi v_\xi)\frac{\partial h_1}{\partial\eta}+\frac{\mu}{h_1}\left[\frac{\partial}{\partial\xi}\left(\frac{v_\xi}{h_1}\frac{\partial h_1}{\partial\eta}\right)-\left(\frac{1}{h_1}\frac{\partial v_\xi}{\partial\xi}-\frac{v_\eta}{h_1}\frac{\partial h_1}{\partial\eta}\right)\frac{\partial h_1}{\partial\eta}\right]$$

3. Flow Solver Development and Verification

The solution algorithm used in the present work is based on the SIMPLER algorithm developed by Patankar (1980) in conjunction with Crank-Nicolson time integration method.

The flow geometry along with the boundary conditions is shown in Fig. 2(a). The outer boun-

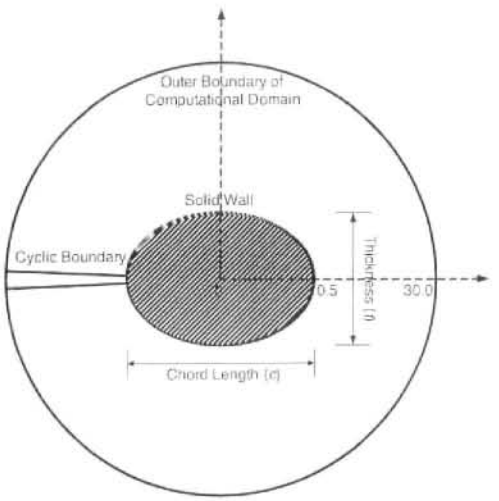

(a) Flow geometry and boundary conditions

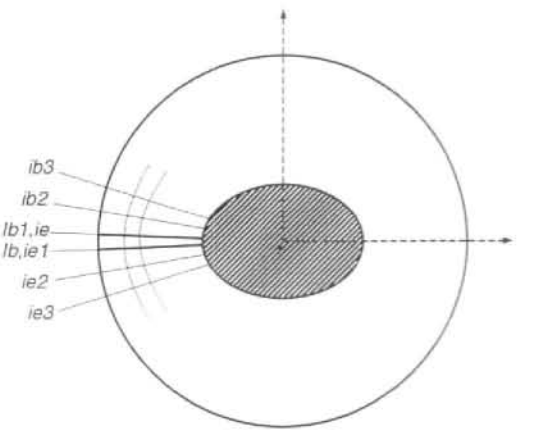

(b) Cell diagram with a cyclic boundary in ξ-direction

Fig. 2 Flow geometry and computational domain

Table 1 Comparisons with available numerical and experimental data ($t/c=1.0$)

Re	Contributor	St	$\overline{Cd}$	ΔCd	ΔCl	$\overline{Cpb}$	ΔCpb
200	present	0.186	1.12	0.03	0.54	−0.78	0.09
	Rogers, Kwak (†)	0.185	1.23	0.05	0.65		
	Belov (†)	0.193	1.19	0.04	0.64		
	Linnick, Fasel (2003)	0.197	1.34	0.04	0.69		
	Berger* (1972)	0.18−0.19					
400	present	0.204	1.07	0.05	0.72	−0.91	0.17
	Jordan, Fromm (1972)	0.200	1.23	0.07	0.75	-1.01	0.16
	Gerrard* (††)					-0.85	
1,000	present	0.219	1.04	0.08	0.88	−1.07	0.27
	Goldstein* (†††)	0.220	1.00				
	Jordan, Fromm (1972)	0.206	1.24	0.12	0.95	−1.15	0.30
	Gerrard* (††)					−0.75	
	Roshko* (††††)	0.210					

Note : 1. (*) denotes experimental results
2. (†) in Linnick and Fasel (2003)
3. (††) in Jordan and Fromm (1972)
4. (†††) in Chou and Huang (1996)
5. (††††) in Mittal and Balachandar (1996)

dary of the computational domain has 30 times of unit chord length distance from the center of an elliptic cylinder. Here, the chord is defined as a straight line connecting the leading edge and trailing edge of the cylinder. The no-slip boundary conditions are imposed on the solid surface and the free stream conditions are applied to the inflow boundary conditions. The outflow boundary conditions are extrapolated from the interior grid point values.

A cyclic boundary condition is implemented to see the unsteady flow physics. A diagram for cyclic boundary is presented in Fig. 2(b). The domain extends from cell $ib1$ to $ie1$ with cell ib overlapping with cell iei and cell ie overlapping with cell $ib1$. Therefore, throughout all the geometry calculations, all geometry parameters needs to be copied from $ib1$ to ie and from $ie1$ to ib. The O-mesh shaped 148×151 grid is generated algebraically.

Not many studies have been performed in the area of unsteady flow past elliptic cylinders. So, the flow solver verification was done by comparing the present numerical solutions with currently available numerical and experimental data for a flow passed a circular cylinder. Table 1 summarizes this comparison result and shows a good agreement.

4. Numerical Results and Discussions

When vortex shedding occurs alternately behind a circular cylinder, a periodic and asymmetric flow pattern is formed. The periodic forces, therefore, act on the circular cylinder in the free stream direction (drag) and normal direction to the free stream (lift). The drag and lift forces exerted on the cylinder may be decomposed into pressure force and friction force components as follows:

$$Cd=Cdp+Cdf,\ Cl=Clp+Clf$$

Here, Cdp and Cdf are the pressure and friction components of the drag coefficient, and Clp and Clf are the pressure and friction components of the lift coefficient, respectively.

Figure 3 shows typical time variations of Cl and Cd as a function of T for the circular cylinder at $Re=200$. Here, the lift and drag coefficients, Cl and Cd, are defined respectively as $Cl=2L/(\rho u_\infty^2 d)$ and $Cd=2D/(\rho u_\infty^2 d)$, where L, D, and d are the lift force per unit span, drag force per unit span, and the cylinder diameter, respectively. Also, the dimensionless time T is defined as $T=\dfrac{t}{d/u_\infty}$, where t is dimensional time. In this figure, oscillating frequencies and amplitudes of both coefficients can be compared very clearly. The amplitude of Cl is much greater than that of Cd, and the frequency of Cl is one-

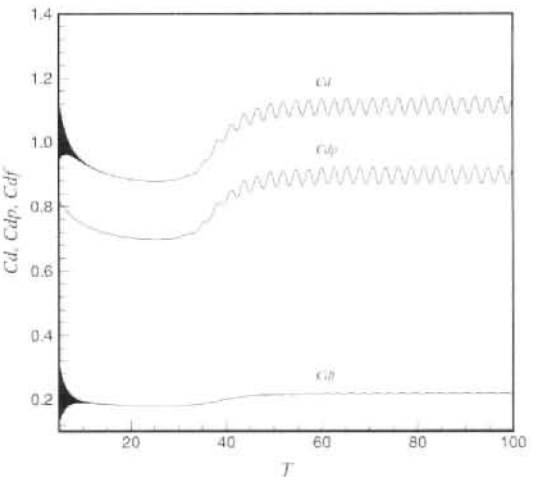

(a) Drag coefficient

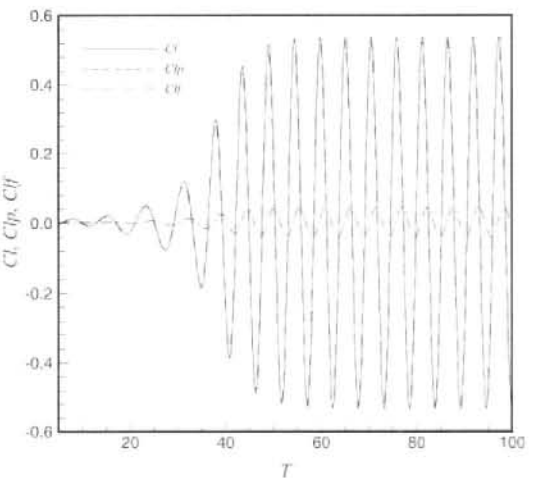

(b) Lift coefficient

Fig. 3 Time variations of drag and lift coefficients for circular cylinder at $Re=200$

half the frequency of Cd. The frequency of Cl due to the vortex shedding can be expressed by Strouhal number, which is made dimensionless with the free stream velocity and the diameter of the circular cylinder as follows :

$$St=\frac{f\times d}{u_\infty}$$

where f is frequency of lift force oscillation. Also, Fig. 3 shows that the amplitudes of friction force oscillations are much less than the amplitudes of pressure force oscillations for both drag and lift forces.

Figure 4 compares the time-averaged total drag coefficient $\overline{Cd}$, pressure drag coefficient $\overline{Cdp}$, and friction drag coefficient $\overline{Cdf}$ at various thickness-to-chord ratios (t/c) of 0.6, 0.8, 1.0, and 1.2 ellipses with different Re of 200, 400, and 1,000 to investigate the effects of ellipse thickness and Reynolds number on the drag coefficients. The mean drag coefficient $\overline{Cd}$ increases a lot with increase of t/c at the same Re, while it decreases as Re increases when t/c is less than 1.0 at the same t/c. For $t/c=1.2$, $\overline{Cd}$ is almost constant at different Re. The total drag force mostly comes from the pressure drag force and the portion of pressure drag force increases with increase of Re or t/c as shown in Table 2. The $\overline{Cdp}$ decreases slightly as Re increases when t/c is less than 1.0 at the same t/c, while it increases slightly with increase of Re when t/c is greater than 1.0. However, $\overline{Cdp}$ has a big increase of its magnitude as t/c increases for the entire range of Reynolds numbers considered in this study. It means that $\overline{Cdp}$ strongly depends on the t/c rather than Re. This figure also shows that the rate of increment of $\overline{Cdp}$ along with increase of t/c is larger when Re is larger.

On the other hand, $\overline{Cdf}$ decreases as Re increases at the same t/c, while its magnitude is an almost same value for the different t/c at the same Re. It means that $\overline{Cdf}$ is hardly affected by

Table 2 The contributing portion of $\overline{Cdp}$ and $\overline{Cdf}$ to the $\overline{Cd}$

Re	t/c	$\overline{Cdp}$ (%)	$\overline{Cdf}$ (%)	Coef. of $\overline{Cd}$
200	0.6	62.1	37.9	0.57
	0.8	73.4	26.6	0.81
	1.0	80.4	19.6	1.12
	1.2	85.1	14.9	1.48
400	0.6	68.5	31.5	0.46
	0.8	79.5	20.5	0.73
	1.0	85.7	14.3	1.07
	1.2	89.4	10.6	1.47
1000	0.6	76.4	23.6	0.37
	0.8	86.2	13.8	0.66
	1.0	90.9	9.1	1.04
	1.2	93.4	6.6	1.47

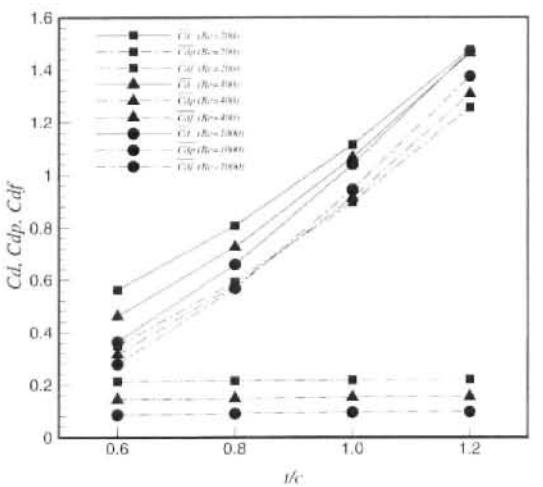

Fig. 4 $\overline{Cd}$, $\overline{Cdp}$, and $\overline{Cdf}$ comparisons at different Re and t/c

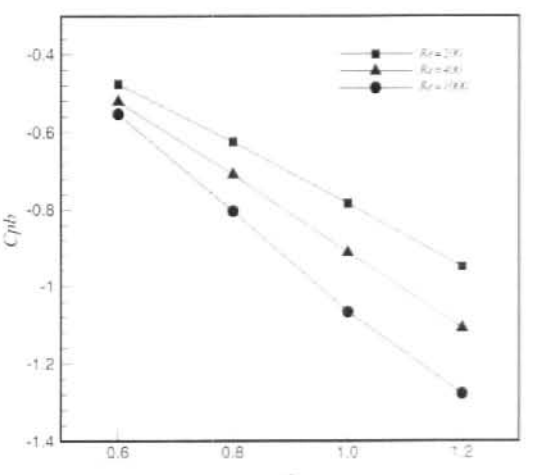

Fig. 5 $\overline{Cpb}$ versus t/c at different Re

the cylinder thickness but strongly affected by Re. Namely, $\overline{Cdf}$ strongly depends on Re.

Time-averaged base pressure coefficient, $\overline{Cpb}$, which is defined as a mean value of Cp at the trailing edge of the cylinder, is plotted with respect to t/c at different Re in Fig. 5. The absolute value of $\overline{Cpb}$ increases as either t/c or Re increases. Actually, the absolute value of $\overline{Cpb}$ becomes bigger when the wake region becomes enlarged because of earlier separation occurrence on the elliptic cylinder surface.

Figure 6 investigates the amplitude of base pressure coefficient, ΔCpb, and the amplitude of leading edge pressure coefficient, ΔCps, at various with different Re. While Δcps is nearly zero value no matter what t/c or Re, the ΔCpb increases as either t/c or Re increases. Although Cp fluctuation at the leading edge is under the influence of Cp fluctuation at the trailing edge, the amplitude ΔCps, which is about the order of 10^{-3}, is much less than ΔCpb.

The amplitudes of Cl and Cd oscillations are one of the very important physics in unsteady flow problem. At the beginning of this section, we already mentioned that the amplitude of Cl is much greater than that of Cd. Fig. 7 investigates the amplitude of Cl and Cd at different Re and t/c. Here, the amplitudes of Cl and Cd oscillations are defined, respectively, as

$$\Delta Cl = \frac{(Cl)_{\max} - (Cl)_{\min}}{2}$$

$$\Delta Cd = \frac{(Cd)_{\max} - (Cd)_{\min}}{2}$$

where the subscripts min and max denote the minimum and maximum values, respectively, in a period. Both ΔCd and ΔCl increase as Re or t/c increases although ΔCd is much less than ΔCl.

Figure 8 plots ΔCl, ΔClp, and ΔClf as a function of t/c with different Re, and Fig. 9 plots ΔCd, ΔCdp, and ΔCdf as a function of

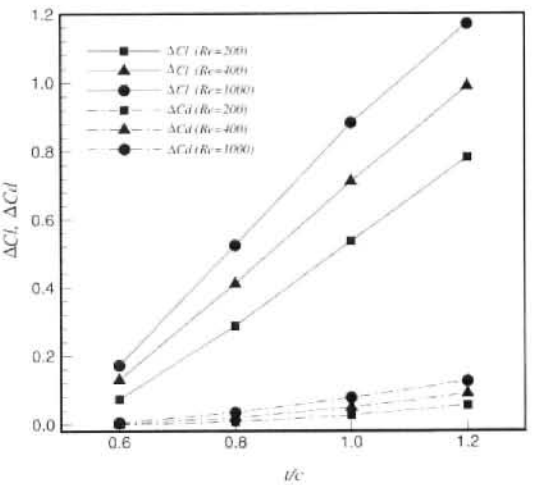

Fig. 7 Effects of Re and tc on ΔCl and ΔCd

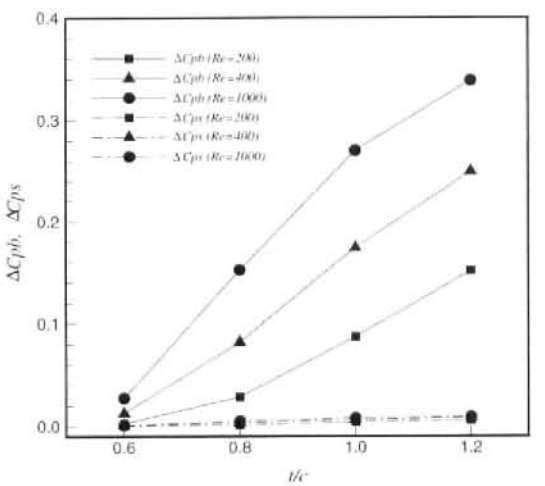

Fig. 6 Effects of Re and t/c on ΔCpb and ΔCps

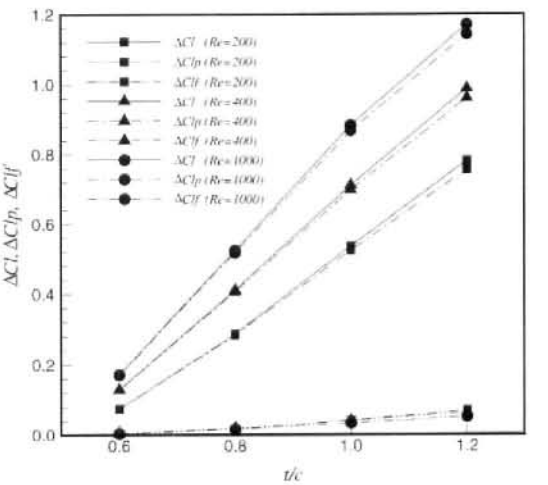

Fig. 8 Effects of Re and t/c on ΔCl, ΔClp, and ΔClf

t/c with different Re. The amplitudes of lift and drag coefficient due to pressure force are denoted as ΔClp and ΔCdp, and the amplitudes of lift and drag coefficient due to friction force are denoted as ΔClf and ΔCdf respectively. Here, note that $\Delta Cl \neq \Delta Clp + \Delta Clf$, $\Delta Cd \neq \Delta Cdp + \Delta Cdf$ because the maximum amplitudes of force oscillations for pressure and friction components do not occur simultaneously. It is clear that $\Delta Cl \cong \Delta Clp$ and $\Delta Cd \cong \Delta Cdp$ because the total drag force mostly comes from the pressure drag force as mentioned already. The ΔCl, ΔClp, and ΔClf increase almost linearly with the increase of t/c for all the different Re, however, ΔCdp shows the parabolic increment tendency as t/c increases for all the different Re.

Figure 10 plots the St as a function of Re for the different t/c. As the Re increases, the vortex shedding frequency increases for all t/c, and the rate of increment of frequency along with the increase of Re is larger when t/c is smaller. The frequency is reduced as t/c increases at the same Re. In other words, the frequency of the vortex shedding is higher when the thickness of elliptic cylinder becomes thinner.

Figsures 11(a) and 11(b) show the development

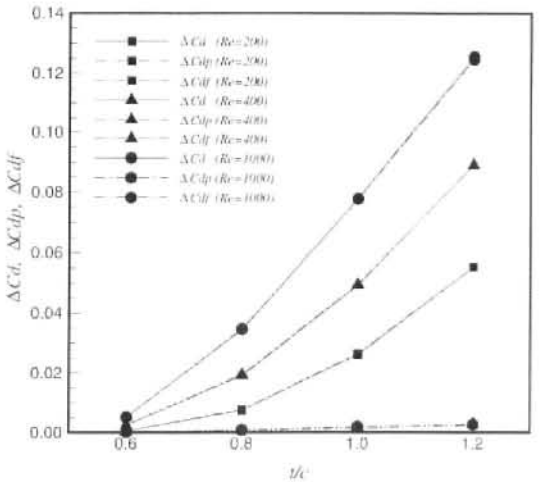

Fig. 9 Effects of Re and t/c on ΔCd, ΔCdp, and ΔCdf

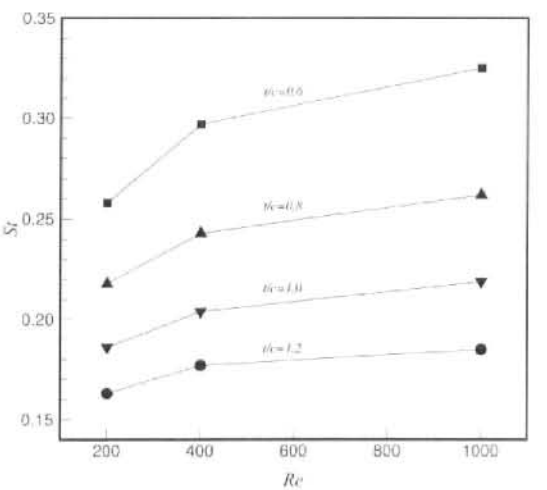

Fig. 10 St versus Re at different t/c

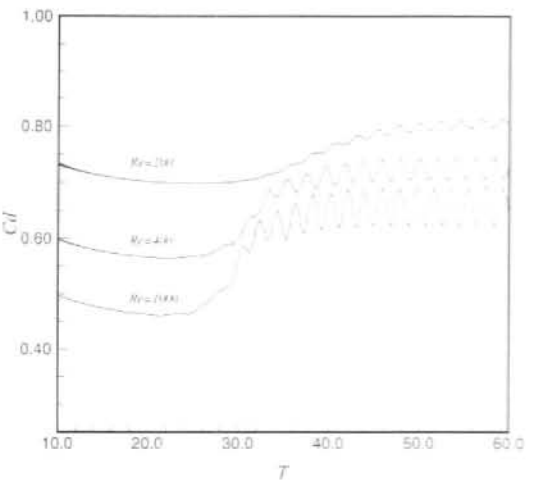

(a) The development of Cd with time for $t/c=0.8$

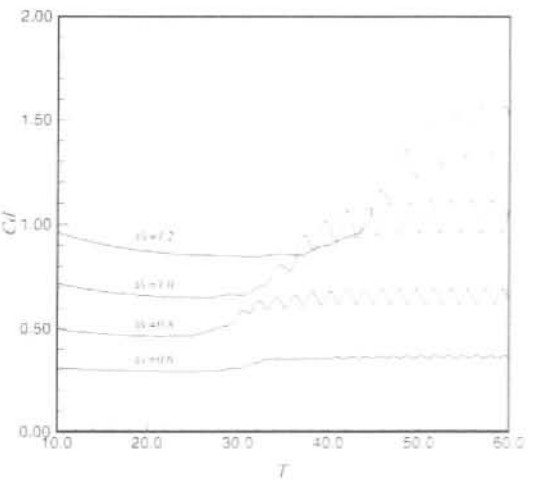

(b) The development of Cd with time at $Re=1000$

Fig. 11 The development of Cd with time

of Cd with time for $t/c=0.8$ at different Re and for different t/c at $Re=1000$, respectively. In these figures, it is observed that the onset of asymmetry is numerically developed faster when the cylinder thickness becomes thinner or Reynolds number becomes larger.

5. Summary and Conclusion

Through this study, we found that the total drag force is increasing a lot with increase of t/c and mostly comes from the pressure drag force. The contributing portion of the pressure drag force is increasing more and more as Re or t/c is increasing. Also, the results show that the mean pressure drag force strongly depends on the cylinder thickness, whereas the mean friction drag force is strongly dependent of the Reynolds number. Additionally, it is found that the rate of increment of the mean pressure drag force along with the increase of cylinder thickness is larger when the Reynolds number is larger.

The amplitudes of lift and drag force oscillations increase with increase of Reynolds number or cylinder thickness although the amplitude of drag force is much less than that of lift force. While ΔClp increases almost linearly with the increase of t/c for all the different Re, ΔCdp increases parabolically.

Not only the absolute magnitude of the mean base pressure but also the amplitude of base pressure oscillation increase as Reynolds number or cylinder thickness increases. Though the Cp fluctuation at the leading edge is influenced by the Cp fluctuation at the trailing edge, the fluctuating magnitude at the leading edge is very small compared with the fluctuating magnitude at the trailing edge.

The frequency of vortex shedding increases as either Reynolds number increases or cylinder thickness decreases, and the rate of increment of frequency along with the increase of Reynolds number is larger when the cylinder thickness becomes thinner. Also, the onset of computed asymmetry around the body is developed faster when the cylinder thickness becomes thinner or Reynolds number becomes larger.

Finally, we conclude that the Reynolds number and cylinder thickness affect significantly the characteristics of the drag and lift forces: mean value, fluctuation amplitude, and oscillating frequency.

Acknowledgments

The authors are grateful to Prof. Ganesh R. Rajagopalan of Iowa State University, Ames for many valuable discussions on this subject.

References

Badr, H. M., Dennis, S. C. R. and Kocabiyik, S., 2001, "Numerical Simulation of the Unsteady Flow Over an Elliptic Cylinder at Different Orientations," *International Journal for Numerical Methods in Fluids*, Vol. 37, pp. 905~931.

Berger, E. and Wille, R., 1972, "Periodic Flow Phenomena," *Ann. Rev. Fluid Mech.*, Vol. 4, pp. 313~340.

Blackburn, H. M. and Henderson, R. D., 1999, "A Study of Two-Dimensional Flow Past an Oscillating Cylinder," *Journal of Fluid Mechanics*, Vol. 385, pp. 255~286.

Chou, M. H. and Huang, W., 1996, "Numerical Study of High-Reynolds-Number Flow Past a Bluff Object," *International Journal for Numerical Methods in Fluids*, Vol. 23, pp. 711~732.

D'Alessio, S. J. D., Dennis, S. C. R. and Nguyen, P., 1999, "Unsteady Viscous Flow Past an Impulsively Started Oscillating and Translating Elliptic Cylinder," *Journal of Engineering Mathematics*, Vol. 35, pp. 339~357.

Jordan, S. K. and Fromm, J. E., 1972, "Oscillatory Drag, Lift, and Torque on a Circular Cylinder in a Uniform Flow," *Physics of Fluids*, Vol. 15, No. 3, pp. 371~376.

Kang, S. and Choi, H., 1999, "Laminar Flow Past a Rotating Circular Cylinder," *Physics of Fluids*, Vol. 11, No. 11, pp. 3312~3321.

Lim, C. K., 1991, "Numerical Simulation of Non-lifting Flow Over Two-dimensional Elliptic Cylinders," MS Thesis, Iowa State University.

Linnick, M. N. and Fasel, H. F., 2003, "A High-Order Immersed Boundary Method for

Unsteady Incompressible Flow Calculations," *AIAA Paper* 2003-1124

Manzari, M T, 2003, "A Time-accurate Finite Element Algorithm for Incompressible Flow Problems," *International Journal of Numerical Methods for Heat & Fluid Flow*, Vol 13, No 2, pp 158~177

Mittal, R and Balachandar, S., 1996, "Direct Numerical Simulation of Flow Past Elliptic Cylinders," *Journal of Computational Physics*, Vol 124, pp 351~367

Nair, M T and Sengupta, T K, 1996, "Onset of Asymmetry Flow Past Circular and Elliptic Cylinders," *International Journal for Numerical Methods in Fluids*, Vol. 23, pp 1327~1345

Nair, M T and Sengupta, T K, 1997, "Unsteady Flow Past Elliptic Cylinders," *Journal of Fluids and Structures*, Vol 11, pp 555~595

Ota, T, Nishiyama, H and Taoka, Y, 1987, "Flow Around an Elliptic Cylinder in the Critical Reynolds Number Regime," *Journal of Fluids Engineering*, Vol 109, pp 149~155

Park, D S., Ladd, D M. and Hendricks, E W, 1994, "Feedback Control of von Karman Vortex Shedding Behind a Circular Cylinder at Low Reynolds Numbers," *Physics of Fluids*, Vol 6, No 7, pp 2390~2405

Park, J, Kwon, K. and Choi, H, 1998, "Numerical Solutions of Flow Past a Circular Cylinder at Reynolds Number up to 160," *KSME International Journal*, Vol 12, No 6, pp 1200~1205

Patankar, S V, 1980, "Numerical Heat Transfer and Fluid Flow," Hemisphere, New York

Patankar, S V and Spalding, D A, 1972, "A Calculation Procedure for Heat, Mass and Momentum Transfer in Three-Dimensional Parabolic Flows," *International Journal of Heat and Mass Transfer*, Vol 15, pp 1787~1806

Patel, V A, 1981, "Flow Around the Impulsively Started Elliptic Cylinder at Various Angles of Attack," Computers and Fluids, Vol 9, No 4, pp 435~462

Perry, A E, Chong, M S and Lim, T T, 1982, "The Vortex-Shedding Process Behind Two-Dimensional Bluff Bodies," *Journal of Fluid Mechanics*, Vol 116, pp 77~90

Sengupta, A, 2003, "Numerical Simulation of Unsteady Incompressible Flow Passed Two-Dimensional Elliptic Cylinders," MS Thesis, Iowa State University

Williamson, C H K, 1996, "Vortex Dynamics in the Cylinder Wake," *Annual Review of Fluid Mechanics*, Vol 28, pp 477~539